Environment International 117 (2018) 215–225

Contents lists available at ScienceDirect

Environment International

journal homepage: www.elsevier.com/locate/envint

Escalating heat-stress mortality risk due to global warming in the Middle East and North Africa (MENA)

Ali Ahmadalipour*, Hamid Moradkhani

Center for Complex Hydrosystems Research, Department of Civil, Construction, and Environmental Engineering, The University of Alabama, Tuscaloosa, AL 35487, United States

ARTICLE INFO

Handling Editor: Olga-Ioanna Kalantzi

Keywords:
Climate change
Mortality
Middle East and North Africa (MENA)
CORDEX
RCM
Wet-bulb temperature

ABSTRACT

Climate change will substantially exacerbate extreme temperature and heatwaves. The impacts will be more intense across the Middle East and North Africa (MENA), a region mostly characterized by hot and arid climate, already intolerable for human beings in many parts. In this study, daily climate data from 17 fine-resolution Regional Climate Models (RCMs) are acquired to calculate wet-bulb temperature and investigate the mortality risk for people aged over 65 years caused by excessive heat stress across the MENA region. Spatially adaptive temperature thresholds are implemented for quantifying the mortality risk, and the analysis is conducted for the historical period of 1951–2005 and two future scenarios of RCP4.5 and RCP8.5 during the 2006–2100 period. Results show that the mortality risk will increase in distant future to 8–20 times higher than that of the historical period if no climate change mitigation is implemented. The coastal regions of the Red sea, Persian Gulf, and Mediterranean Sea indicate substantial increase in mortality risk. Nonetheless, the risk ratio will be limited to 3–7 times if global warming is limited to 2 °C. Climate change planning and adaptation is imperative for mitigating heat-related mortality risk across the region.

1. Introduction

Global warming will increase the frequency and intensity of heatwaves and extreme high temperatures (Fischer and Knutti, 2015; Mora et al., 2017; Pal and Eltahir, 2016). Even if the global mean temperature increase is limited to 2 °C, the warming over land will be far beyond 2 °C in many regions (Coffel et al., 2017; Fischer et al., 2013; King et al., 2017). The social impacts of climate change and extreme temperatures garnered more attention after the 2003 European heatwave which caused high mortality (Christidis et al., 2015; Li et al., 2016). The ongoing anthropogenic temperature rise has raised serious concerns regarding human health (Kingsley et al., 2016; Mitchell et al., 2016; Williams et al., 2012) and economy (Dunne et al., 2013; Underwood et al., 2017; Zander et al., 2015; Zhao et al., 2016). Climate change has already prolonged the heatwaves and increased their frequency in various locations of the world (Sun et al., 2014). The severe heatwaves of Texas in 2011 (Luo and Zhang, 2012), Australia in 2012 (Lewis and Karoly, 2013), China in 2015 (Miao et al., 2016), and Egypt in 2015 (Mitchell, 2016) were all experienced at large spatial extent and prolonged duration.

The anthropogenic warming in MENA is strongest in summer; whereas elsewhere it is usually stronger in winter (Lelieveld et al., 2016; Waha et al., 2017). Considering the hot arid climate of the majority of MENA region, the morbidity and mortality risk of extreme high temperatures is one of the grand challenges facing human health and society (Russo et al., 2016). Studies have demonstrated that climate change will increase air temperature across the Middle East to thresholds not tolerable for human body, especially around the Persian Gulf (Im et al., 2017; Pal and Eltahir, 2016). Schär (2016) discussed that the air temperature has already exceeded the postulated tolerance threshold in some humid areas around the Persian Gulf (e.g. Bandar Mahshahr, Iran).

When exposed to hot temperatures, human body dissipates heat by sweating and increasing heart rate in order to increase blood flow to the body surface, which in turn reduces the oxygen supply to muscles and brain. In addition, dehydration increases the blood viscosity and makes it harder for the heart to circulate it. The physiological processes caused by increased core body temperature result in mental and physical fatigue, and augment the likelihood of exhaustion, heart attack, and mortality (Kjellstrom et al., 2016; Loughnan et al., 2010; Ross et al., 2018). Accordingly, multitude of studies have projected significant increase in heat-related morbidity and mortality by the end of 21st century due to exposure to higher ambient temperatures (Chen et al., 2017; Ostro et al., 2012; Peng et al., 2011; Weinberger et al., 2017).

* Corresponding author.
E-mail address: aahmada@ua.edu (A. Ahmadalipour).

https://doi.org/10.1016/j.envint.2018.05.014
Received 12 February 2018; Received in revised form 4 May 2018; Accepted 6 May 2018
Available online 12 May 2018

Several studies have investigated the mortality risk caused by extreme temperatures, some of which merely focused on the relationship (mostly linear correlation) between the global warming rate and the changes in mortality (Huber et al., 2017; Mazdiyasni et al., 2017). It has been discussed that climate change is not the only cause for mortality, and that heat-related mortality may occur at any time and any location (Loughnan et al., 2010; WHO, 2014). Therefore, health risk models have been developed in recent years to quantify the heat-related mortality risk and the impacts of climate change on it (Honda et al., 2014; Loughnan et al., 2012; Merte, 2017). The current study investigates the impacts of climate change on mortality risk of people aged over 65 years using a recently developed health risk model.

Dry-bulb temperature (simply referred to as temperature) is different from the temperature that the body feels. Humidity, radiation, and wind speed are among the factors influencing the real-feel temperature that human body experiences (Knutson and Ploshay, 2016; Willett and Sherwood, 2012). Therefore, wet-bulb temperature (TW) has been proposed as a proxy of the real-feel temperature, and it has been utilized as a measure for human discomfort (Dunne et al., 2013). The primary benefit of utilizing TW rather than dry-bulb temperature is that TW better represents the real-feel temperature that human body experiences (Mitchell et al., 2016; Pal and Eltahir, 2016; Willett and Sherwood, 2012). Moreover, TW is more confined compared to the dry-bulb temperature and it is more reliable for assessing human health-related issues (Raymond et al., 2017; Zhao et al., 2016).

Despite the multitude of heat-related mortality assessments, a comprehensive and rigorous analysis of climate change impacts on mortality risk of the MENA region is missing. Many of the previous analyses either employed a simplified methodology, utilized coarse resolution (temporal and spatial) data, or focused on a limited study period. The application of raw air temperature data, rather than the more reliable wet bulb temperature, is another deficit in many previous analyses. Moreover, uncertainty is an intrinsic feature of climate change assessments, and accurate characterization of the uncertainty helps providing more reliable projections, which will be beneficial for mitigation planning purposes (Ahmadalipour et al., 2018). Inaccurate representation of the climate change uncertainties is a common shortcoming of many previous assessments, and that is generally caused by limited number of climate models and scenarios employed as well insufficient parameterization of the impact model used (Ahmadalipour et al., 2017a; Rana et al., 2017).

The current study investigates the impacts of global warming on the mortality risk of people over 65 years of age caused by extreme high temperatures. A large ensemble of regional climate models (RCMs) is employed to calculate daily TW across the MENA. The mortality risk is then quantified using a recently developed health risk model, and the impacts of climate change on the mortality risk are investigated. The data, models, and methodology are explained in the next sections, followed by results and discussion.

2. Study area and data

The study area is located between the latitudes 6.6°S–42°N and longitudes 20°W–60°E covering parts of 70 countries and accommodating over 600 million inhabitants. The climate of the region is mostly characterized by hot arid areas with very low precipitation (Waha et al., 2017). The Sahara Desert in northern Africa and parts of the Middle East are among the driest regions in the globe (Hameed et al., 2018). However, the study region consists of very humid regions as well, and humidity variations have substantial effect on the real-feel temperature. To better understand spatial variations of humidity across the study region, the historical mean relative humidity across the MENA region is extracted and plotted in Supplementary Fig. S1. Almost half of the study area indicates mean relative humidity > 40%, especially in coastal regions and also the central Africa.

Daily maximum near surface temperature (Tx) and relative humidity (hurs) are acquired during summer (June, July, and August) for 17 RCMs. For climate data, we utilized RCMs developed by the Coordinated Regional Climate Downscaling Experiment (CORDEX) (Jones et al., 2011). The CORDEX RCMs are developed at 14 different domains across the globe, two of which cover the MENA region (i.e. MNA and AFR). The MNA domain latitude and longitude ranges are [−6.6°S–44.88°N] and [−26.4°W–75.24°E], respectively, and the boundary of AFR domain is [−45.76°S–42.24°N] and [−24.64°W–60.28°E]. All the models from both domains are utilized in this study, and the common boundary of MNA and AFR domains is employed (i.e. [−6.6°S–42.24°N] and [−24.64°W–60.28°E]). Tx and hurs are acquired from the 17 RCMs at a daily temporal resolution and 0.44° spatial resolution for summers during the historical period of 1951–2005 and two future scenarios of RCP4.5 (corresponding to 2 °C global warming by the end of 21st century) and RCP8.5 (business as usual scenario) for the period of 2006–2100. More information about

Table 1
The 17 RCMs used in this study and their characteristics. All the RCMs have a spatial resolution of 0.44° and they are analyzed at a daily temporal resolution.

No.	Deriving GCM	Original modeling institute	Original resolution (lat × lon)	Domain	Ens. member	Downscaling institute[a]	tasmax	hurs
1	CanESM2	Canadian Centre for Climate Modeling and Analysis	2.8° × 2.8°	AFR-44	r1i1p1	SMHI	✓	✓
2	CNRM-CM5	National Centre of Meteorological Research, France	1.4° × 1.4°	AFR-44	r1i1p1	CLM	✓	×
3				AFR-44		SMHI	✓	✓
4				MNA-44		SMHI	✓	✓
5	CSIRO-Mk3-6-0	Commonwealth Scientific and Industrial Research Organization, Australia	1.8° × 1.8°	AFR-44	r1i1p1	SMHI	✓	✓
6	EC-EARTH	EC-EARTH consortium	1.0° × 1.0°	AFR-44	r12i1p1	CLM	✓	×
7				AFR-44	r12i1p1	MPI	✓	×
8				AFR-44	r12i1p1	SMHI	✓	✓
9				MNA-44	r12i1p1	SMHI	✓	✓
10	GFDL-ESM2M	Geophysical Fluid Dynamics Laboratory	2.5° × 2.0°	AFR-44	r1i1p1	SMHI	✓	✓
11				MNA-44	r1i1p1	SMHI	✓	✓
12	IPSL-CM5A-MR	Institut Pierre-Simon Laplace	2.5° × 1.25°	AFR-44	r1i1p1	SMHI	✓	✓
13	MIROC5	Atmosphere and Ocean Research Institute (The University of Tokyo), National Institute for Environmental Studies, and Japan Agency for Marine-Earth Science and Technology	1.4° × 1.4°	AFR-44	r1i1p1	SMHI	✓	✓
14	MPI-ESM-LR	Max Planck Institute for Meteorology (MPI-M)	1.9° × 1.9°	AFR-44	r1i1p1	CLM	✓	×
15					r1i1p1	MPI	✓	×
16					r1i1p1	SMHI	✓	✓
17	NorESM1-M	Norwegian Climate Centre	2.5° × 1.9°	AFR-44	r1i1p1	SMHI	✓	✓

[a] SMHI: Swedish Meteorological and Hydrological Institute; CLM: Climate Limited-area Modeling Community.

the RCMs used in this study is provided in Table 1. To better understand the differences between the two scenarios (i.e. RCP4.5 and RCP8.5), the global monthly mean air temperature data are acquired from the corresponding global climate models, and the decadal global mean temperature rise (compared to the pre-industrialized era) is shown in Supplementary Fig. S2.

For the observation, the Climate Research Unit (CRU) dataset is utilized for the period of 1951–2016 at a monthly timescale and 0.5° spatial resolution (Harris et al., 2014). Due to lack of reliable daily fine-resolution observation data across the region, the monthly observations of CRU (the finest temporal resolution for CRU dataset) are utilized for validation purposes. Moreover, daily climate data from the ERA-interim reanalysis are acquired for the period of 1979–2015 at 0.4° spatial resolution (Dee et al., 2011). To ensure spatial consistency, both the observed and reanalysis data are interpolated to 0.44° spatial resolution using a bilinear interpolation technique.

3. Methodology

3.1. Calculating wet-bulb temperature (TW)

The first step of the analysis is to calculate daily TW. To do so, an empirical equation developed by Stull (2011) is employed, which is based on air temperature and relative humidity, as follows:

$$T_w = T \times \operatorname{atan}\left[0.151977(RH\% + 8.313659)^{\frac{1}{2}}\right] + \operatorname{atan}(T + RH\%) - \operatorname{atan}(RH\% - 1.676331) + 0.00391838(RH\%)^{\frac{3}{2}}\operatorname{atan}(0.023101RH\%) - 4.686035 \quad (1)$$

where T is the dry-bulb air temperature in Celsius, RH% indicates the relative humidity, and T_w is the wet-bulb temperature in Celsius. Wet-bulb temperature can be calculated for any air temperature. In this study, since the objective is on extreme temperature (based on the employed health risk model), TW is calculated using the maximum near-surface air temperature (Tx).

Daily TW is calculated using Eq. (1) for each RCM over the period of 1951–2100. Although more simplified equations have been used for calculating TW in other studies (e.g. Mitchell, 2016), the equation used here has proved to be accurate for temperatures as high as 50 °C and a wide range of relative humidity (5%–99%) (Stull, 2011).

3.2. Quantifying mortality risk

Some of the previous studies considered a constant threshold (e.g. TW > 35 °C) to investigate the health-related risks of climate change (Pal and Eltahir, 2016). However, the physiological attributes of human body and its tolerance to heat is distinct in different regions of the world. For instance, people living in sub-Saharan Africa have been exposed to (and are adapted to) higher temperatures than those living in Northern Canada. Therefore, considering spatially variable temperature threshold seems more logical for reliable assessment of mortality risk.

The methodology for quantifying the impacts of excessive heat on mortality has been recently developed by Honda et al. (2014) and it has been employed by various agencies including the World Health Organization (WHO, 2014). It is based on a comprehensive global analysis of the relationship between mortality and temperature deviation. The implemented health risk methodology is derived based on epidemiological studies analyzing the impacts of temperature on all-cause mortality, including external causes such as deaths from heatstroke and heat-related accidents (WHO, 2014). Honda et al. (2014) showed that the heat-related excessive mortality has the lowest value in an optimum temperature (T_{opt}) and it increases afterwards. The 84th percentile of daily maximum temperature was found the closest proxy of T_{opt} in over 90% of the cities assessed (Honda et al., 2014). Thus in this study, T_{opt} is calculated for each grid of each RCM as the 84th percentile of the historical daily TW. The calculated T_{opt} from each RCM is shown in Fig. 1.

After calculating T_{opt}, the relative mortality risk (RMR) is quantified based on the temperature offset ($\Delta T = T - T_{opt}$) using Eq. (2) as follows (WHO, 2014):

$$RMR = -2.91 \times 10^{-5}\Delta T^3 + 0.00153\Delta T^2 + 0.0054\Delta T + 1 \quad (2)$$

where RMR is the daily relative mortality risk, and it is calculated for each day during the summer. For temperatures below T_{opt}, RMR = 1. The objective of this study is to quantify the excessive mortality risk which is caused by global warming. Thus, similar to WHO (2014), RMR-1 will obtain the excessive mortality risk for each day. If TW of a day is lower than T_{opt}, there will be no excessive heat-stress mortality risk and RMR will be equal to 1 (i.e. RMR-1 = 0 indicating no excessive mortality risk). Therefore, for the days warmer than T_{opt} (days with RMR > 1), the excessive mortality risk (RMR-1) is calculated. It is then aggregated over summer to obtain the summer excessive mortality risk of the year, as follows:

$$\text{Summer Excessive Mortality Risk} = \sum_{n=1}^{N} (RMR_n - 1) \quad (3)$$

where N denotes the number of days (in a particular year) that RMR > 1. Fig. 2 represents the methodology for quantifying mortality risk. The plots a and b indicate the results for Eqs. (2) and (3), respectively. The figure shows that the summer excessive mortality risk of a year is a function of intensity (temperature offset, ΔT) and frequency (number of days warmer than T_{opt}). For instance, in a particular year, if 40 days are ~5 °C warmer than the optimum temperature, the summer excessive mortality risk will be about 2.5.

After calculating the summer excessive mortality risk, it is compared to the historical mean excessive mortality risk to provide the rate of change for mortality risk.

$$(\text{Mortality Risk Ratio})_i|_{i=2006:2100} = \frac{(\text{Summer Excessive Mortality Risk})_i}{\text{Historical Mean Summer Mortality Risk}} \quad (4)$$

The mortality risk ratio indicates the rate that mortality risk will change compared to the historical period. Decadal mean mortality risk ratio is then calculated in order to investigate the long-term impacts of climate change. The methodology is conducted separately for each RCM and each future scenario to characterize the uncertainties.

4. Results

The analysis begins with assessing RCMs' ability in simulating the historical Tx compared to observation and reanalysis. Historical mean summer Tx is calculated for the common period of 1979–2005, and the results are shown in Supplementary Fig. S3. RCMs show acceptable performance compared to the observation for most regions. The fine-scale spatial resolution of RCMs allows them to capture the regional climate characteristics associated with the land cover and elevation patterns fairly well. Comparing CRU and ERA-interim, disparities are found, especially across the central Africa. This is reflected more clearly in Supplementary Fig. S4 when assessing the regional Tx simulations in historical and future periods. Although CRU and ERA-interim are highly correlated, they show about 2 °C difference, with CRU being warmer in most regions except for the Middle East where ERA-interim indicates higher Tx than CRU. In general, historical simulations indicate that RCMs are capable of capturing the long-term trends in all the selected regions.

The lack of accurate and reliable long-term daily observational data at fine spatial resolution is a critical issue across most regions of Africa, which makes the evaluation of climate models a challenge. Due to the unavailability of accurate fine-resolution observations, the RCMs are not bias-corrected in this study. Instead, the methodology is designed

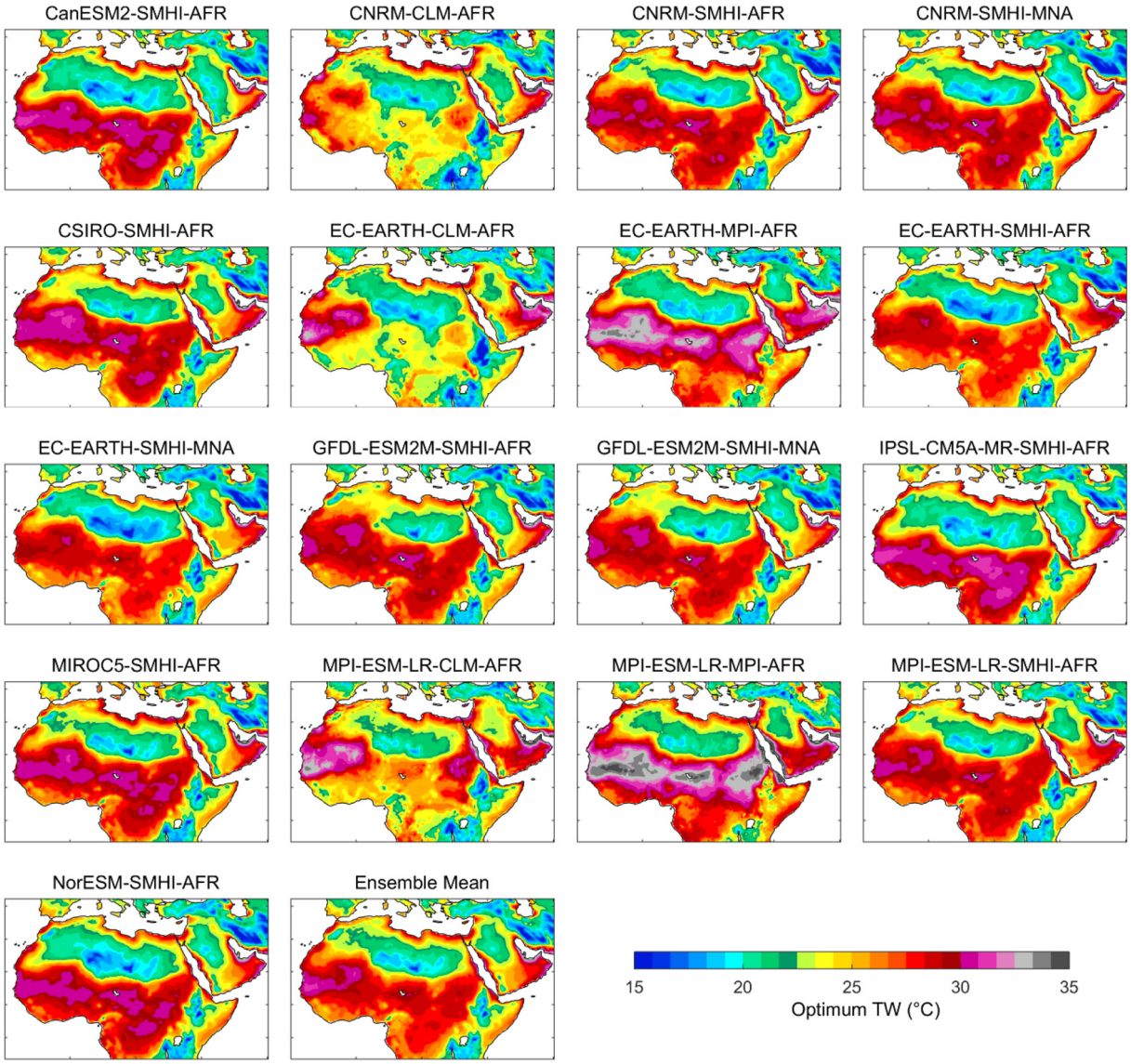

Fig. 1. Optimum wet-bulb temperature (T_{opt}) calculated for each RCM and the ensemble mean (last plot) using the historical data for the period of 1951–2005.

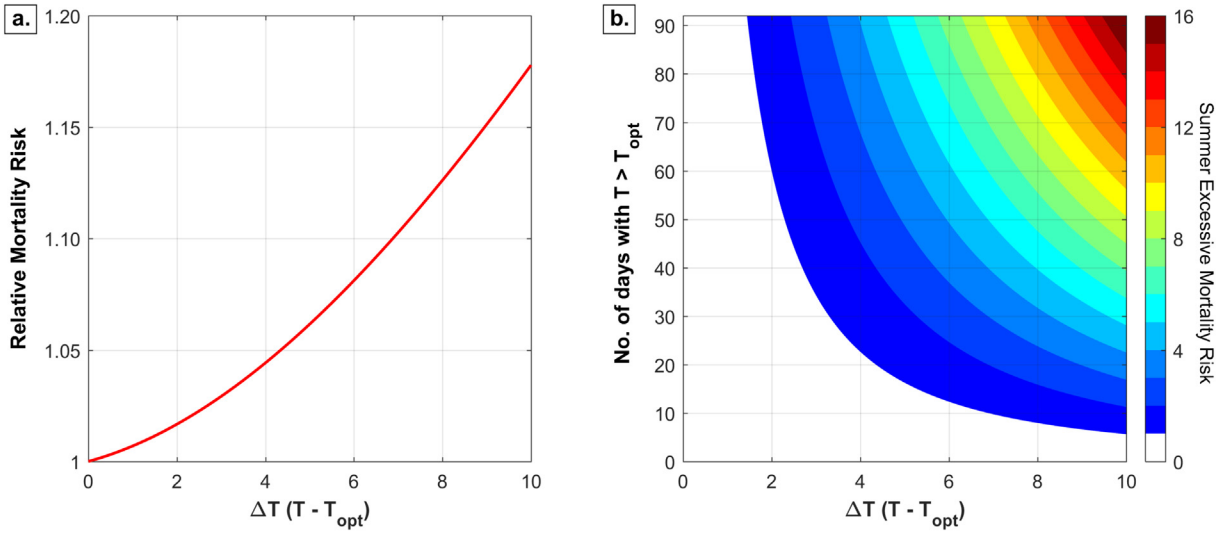

Fig. 2. a) The function used for quantifying the relative mortality risk based on temperature offset (Eq. (2)). b) Summer excessive mortality risk as a function of temperature offset and frequency (Eq. (3)).

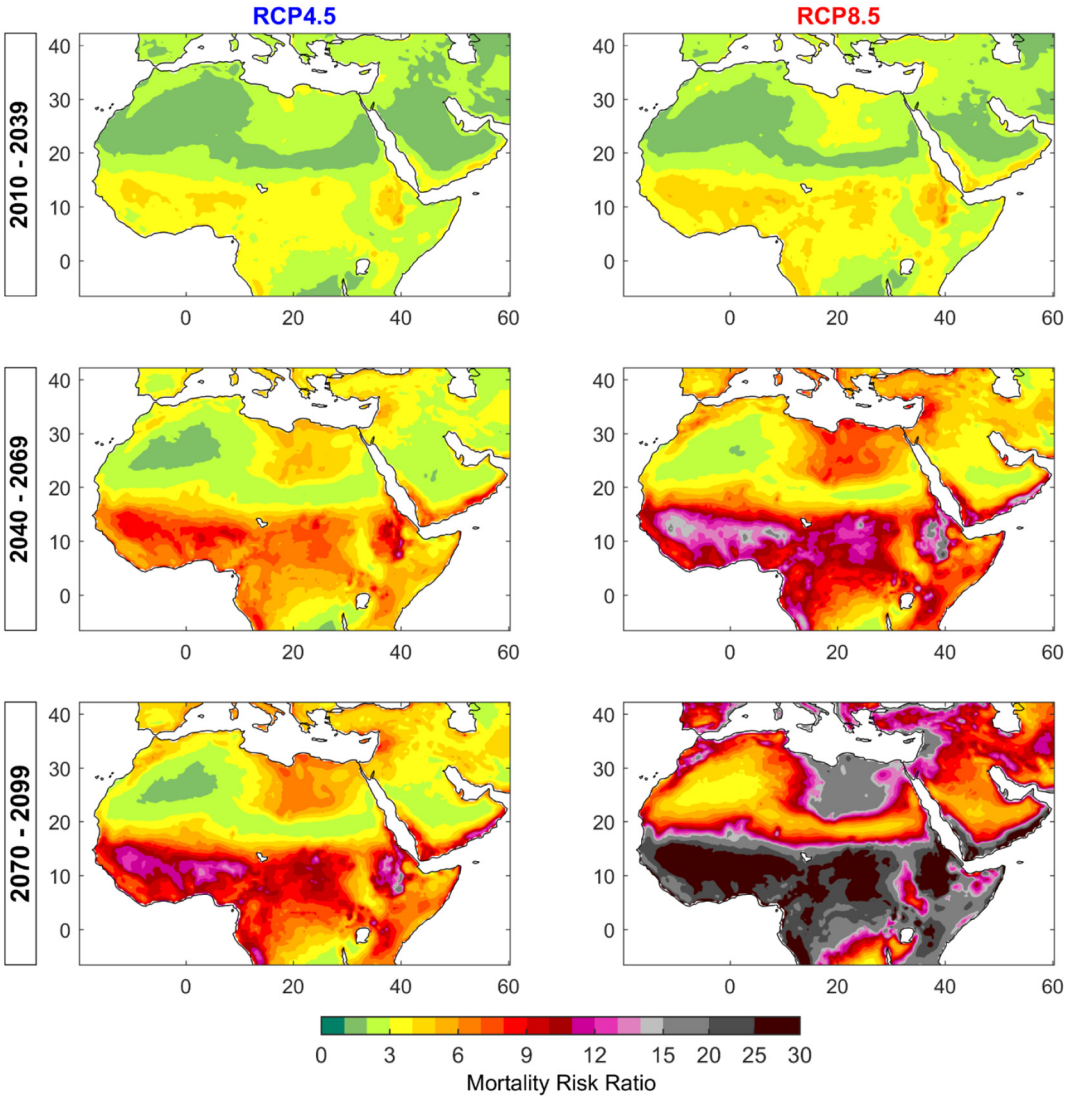

Fig. 3. Projected decadal mortality risk ratio compared to the historical mortality risk. The figure represents the ensemble mean of 17 RCMs and shows the exacerbation rate of mortality risk compared to the historical period.

such that it compares the future projections of each model with its own historical simulations to assess the impacts of climate change. Nonetheless, several previous studies evaluated CORDEX RCMs across Africa and found promising performance for most regions (e.g., Nikiema et al., 2017; Ring et al., 2017).

The mortality risk ratio (Eq. (4)) is quantified for each RCM and each year, and the ensemble mean of 17 RCMs is calculated for 30-year periods of near future (2010–2039), intermediate future (2040–2069), and distant future (2070–2099). The results of mortality risk ratio are plotted in Fig. 3. The figure captures the regional intensification of heat-related mortality risk compared to the historical period. Considering the results of near future (top row), the risk of heat-related mortality over the Middle East is expected to be 2–3 times higher than that of the historical period. The difference between the risk of RCP4.5 and RCP8.5 is negligible in near future and it increases through time, with large disparities in distant future. The figure shows that even if the future global temperature increase is limited to 2 °C (RCP4.5), heat-related mortality risk in western Africa will be about 10 times higher than that of the historical period. However, following a business as usual scenario (RCP8.5), the mortality risk ratio for the same region will be about 30 times higher than the historical risk.

From Fig. 3, the highest mortality risk is found in the areas of western Africa below the Sahara. In general, the southern regions of MENA indicate higher mortality risk ratio compared to northern parts, and there seems to be a latitudinal pattern associated with the risk ratio. In order to investigate the latitudinal patterns, the mortality risk ratio of each RCM is averaged over land at each latitude, and the results are plotted in Fig. 4. In the figure, the results of RCMs are plotted using the shaded area, and the line in the middle represents the ensemble mean of 17 RCMs. The boxplots at the bottom of each plot show the distribution of mortality risk ratio from all models across all latitudes, as a proxy of the mortality risk ratio over MENA in each period. Results for RCP4.5 and RCP8.5 are plotted in blue and red, respectively.

Fig. 4 shows that the highest mortality risk ratio across MENA is found at 12°N (also associated with the highest uncertainty), and both future scenarios indicate similar latitudinal pattern. Considering the interquartile range of the boxplots shown at the bottom of each subplot in Fig. 4, mortality risk ratio of MENA in near future is expected to exceed 2–3 times higher than the historical period, with both concentration pathways indicating similar results. However, in distant future, the interquartile range of the mortality risk ratio will be 3–7 and 8–20 for RCP4.5 and RCP8.5, respectively. In distant future, some of the models indicate risk ratios up to 40 times the historical mortality risk. Furthermore, Fig. 4 shows that although the moderate scenario (RCP4.5) is not much different from the business as usual scenario (RCP8.5) in near future, the latter leads to devastating mortality risks in

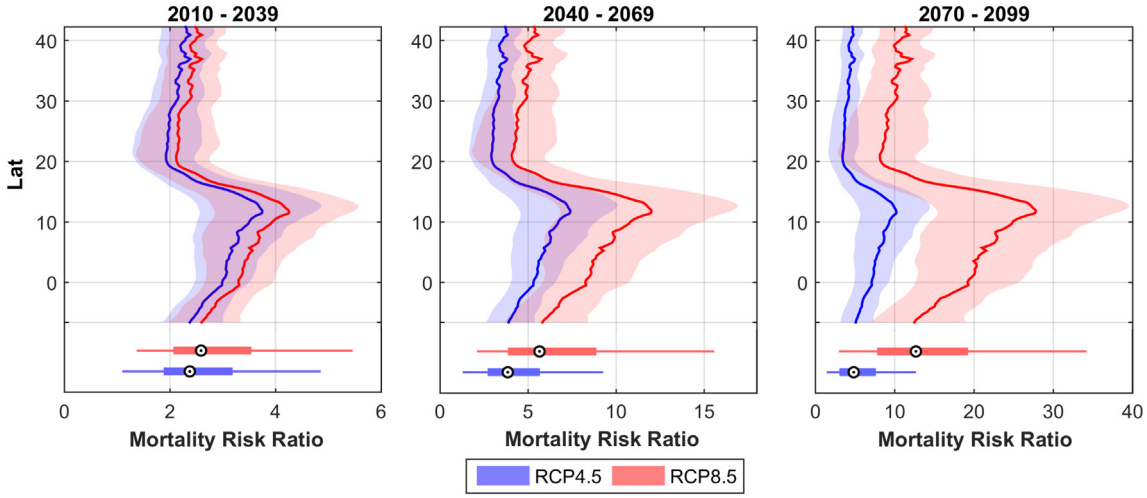

Fig. 4. Latitudinal mean of future mortality risk ratio over land from 17 RCMs (shaded area) and the ensemble mean (bold line) for each 30-year future period. The boxplots at the bottom of each plot indicate the results across the entire MENA region.

distant future. In fact, the highest (least probable) mortality risk ratio from RCP4.5 is lower than the median (most probable) mortality risk projected by RCP8.5 in distant future.

From Fig. 4, the primary source of uncertainty in projected mortality risk is found varying with time and location. In near future, the two scenarios (i.e. RCP4.5 and RCP8.5) indicate similar results, and model uncertainty is found to be the major source of uncertainty. The findings are in agreement with previous attribution of climate change uncertainties (Ahmadalipour et al., 2018; Etemadi et al., 2013). Moreover, the range of uncertainty (the width of shaded area) is similar for the two scenarios and among different latitudes. However, scenario uncertainty is much more considerable in distant future, and in fact, the spread of RCP8.5 is almost beyond that of RCP4.5 in distant future. The model uncertainty in distant future is more noticeable for the latitudes 0–18°N, and it is found considerably lower for latitudes above 30°N. In general, model uncertainty is found to be higher in RCP8.5 than RCP4.5.

Focusing again on Fig. 3, the mortality risk ratio is found to be considerably high in many coastal areas, which is a critical issue for the regions located around the Persian Gulf, Red Sea and the Mediterranean Sea, all of which are among the destinations that millions of tourists visit each year for leisure. In order to better understand the spatial patterns of mortality risk ratio, we first investigate the future temperature changes. Fig. 5 shows the decadal changes of maximum air temperature (ΔTx) and wet-bulb temperature (ΔTW) over land (the top two rows) and water (the bottom two rows). In the figure, the brown and green histograms (the first and third rows) indicate the probability density function (PDF) of the ensemble mean of ΔTx and ΔTW, respectively. Furthermore, the density-type scatterplots (the second and fourth rows) are employed to compare ΔTx and ΔTW from all the 17 RCMs.

Fig. 5 demonstrates the difference between changing patterns of temperature over land and water. From the figure, ΔTx and ΔTW have a linear relationship with similar values over water (the bottom rows). However, ΔTx is always higher than ΔTW over land (the top two rows). In simple words, the changes of dry- and wet-bulb temperature are similar over water, whereas the former is higher than the latter over land (ΔTx over land is higher than that over water). The figure also corroborates that TW is more bounded compared to Tx, and albeit ΔTx may increase up to 6 °C in RCP8.5 of distant future (shown in brown color in the last plot of first row), ΔTW is usually below 4 °C for the same period (shown in green color in the last plot of first row). Moreover, the variability of ΔT (both dry- and wet-bulb) is found to be higher over land than water. The decadal spatial changes of Tx and TW are shown in Fig. 6 to better elaborate on the regional differences. For ΔTx, the highest increase over land is found over the Mediterranean region; whereas for ΔTW, central African regions below the Sahel indicate the highest values.

In order to better understand the projected mortality risk ratio and the influential factors, the second factor affecting mortality, i.e. the frequency, is investigated. To do so, the percentage of days with TW > T_{opt} (frequency of unsafe days) is extracted for each RCM, and the ensemble mean of the results are plotted in Fig. 7. The figure shows that during the historical period, the frequency of unsafe days over land was about 14–18%. The same for near and distant future is about 20–50% and 30–100%, respectively. The combination of ΔTW intensity (Fig. 6) and frequency (Fig. 7) of excessive heat explains the spatial variations of mortality risk ratio (presented in Fig. 3). Results indicate that although the northern latitudes, especially the Mediterranean region, indicate the highest ΔTW among other areas, the mortality risk ratio is highest at lower latitudes, which is similar to the spatial pattern of frequency (Fig. 7).

Results of Fig. 7 indicate apprehensive conditions for frequency of unsafe days in distant future, if no emission mitigation is undertaken (i.e. RCP8.5). The reason for such high frequency can be explained by investigating the variations (intra-annual standard deviation) of temperature, as shown in Supplementary Fig. S5. The figure captures the spatial changes of intra-annual variation of TW, which is then translated to a shift in the frequency of unsafe days. Investigating T_{opt}, ΔTW, and the changes in the frequency (shown in Fig. 1, Fig. 5, and Fig. 7, respectively), it is found that in general, the southwestern parts of MENA indicate the highest T_{opt} and ΔTW as well as substantial increase in the frequency of unsafe days, eventually resulting in the highest mortality risk ratio. To better understand the role of each factor (i.e. intensity and frequency) on mortality risk, consider two cases:

- Case A: 20 unsafe days with ΔTW = 1.5 °C (on average); representing land areas
- Case B: 60 unsafe days with ΔTW = 1.1 °C (on average); representing coastal areas

The Summer Excessive Mortality Risk is calculated according to Eq. (3), and the values for case A and case B are 0.23 and 0.47, respectively. Therefore, although the intensity of case A is 0.4 °C (about 40%) higher than case B, the Summer Excessive Mortality Risk of case B is about twice that of case A, which clearly indicates the role of frequency and intensity for coastal and land areas.

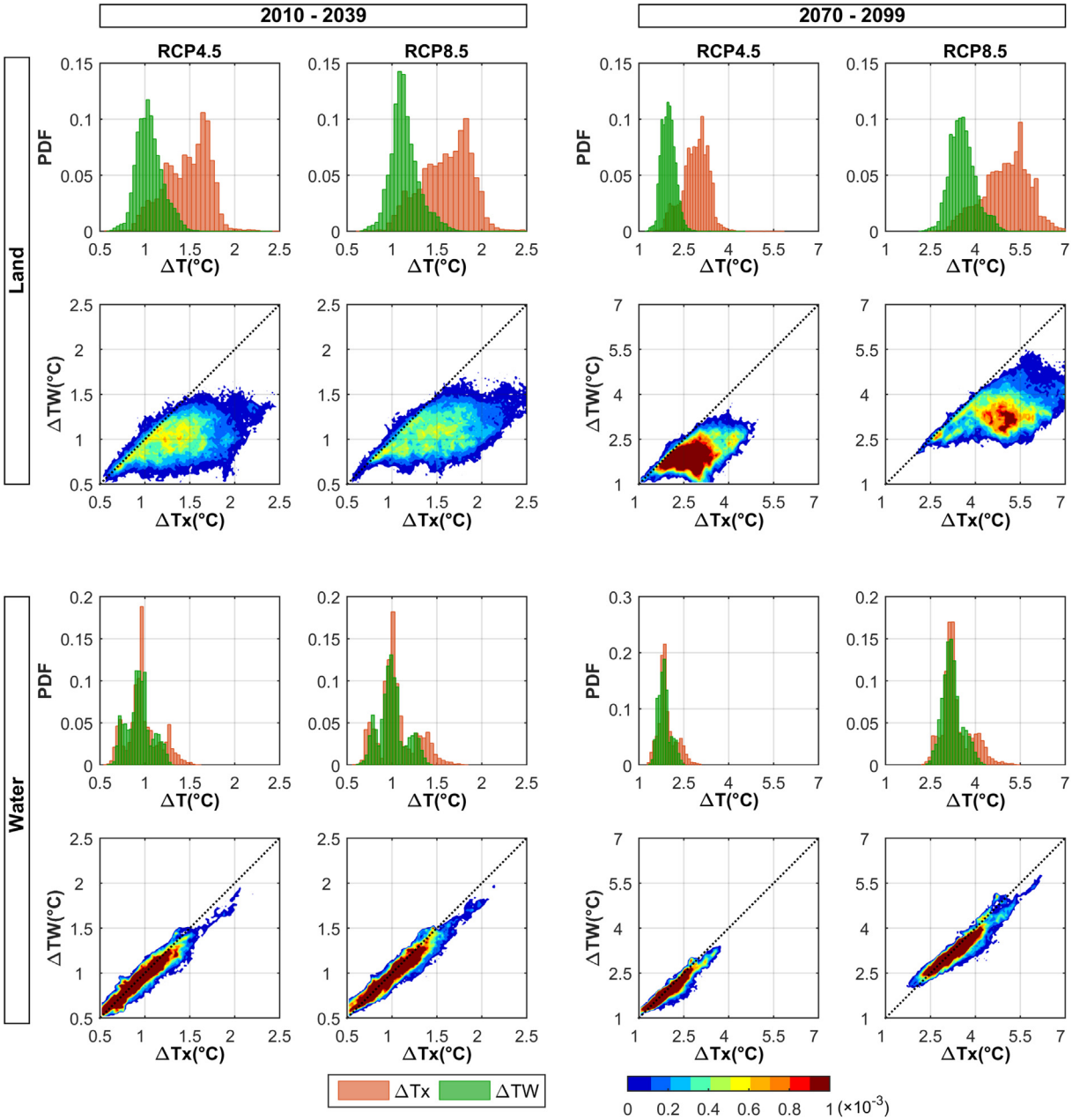

Fig. 5. The change of maximum air temperature (ΔTx) and wet-bulb temperature (ΔTW) across MENA over land (top) and water (bottom). The histogram plots (the first and third rows) show the distribution of the ensemble mean of 17 RCMs. The density-type scatterplots (the second and fourth rows) compare ΔTx and ΔTW of all RCMs, with the color bar indicating the density.

5. Discussion

This study quantified the heat-related mortality risk of people aged 65 and over, and investigated the impacts of climate change on human mortality. Several previous studies analyzed the impacts of climate change on mean and extreme temperature for various parts of the globe (e.g. Coffel et al., 2017; Dosio, 2016; Rana and Moradkhani, 2016). However, fewer studies have investigated the impacts of climate change from a health perspective. It has been shown that the air temperature rise is primarily attributed to the anthropogenic forces exerted by the excessive concentration of greenhouse gases in the atmosphere (Kam et al., 2016; Knutson and Ploshay, 2016; Sun et al., 2017).

It should be noted that although spatially variable T_{opt} was used in this study, no adaptation scenario (i.e. temporally variable T_{opt}) was considered here. This is due to two main reasons: (i) studies have argued that although human body may adapt to dry-bulb temperature to some extent, its adaptation capacity is limited for TW (Pal and Eltahir, 2016); (ii) an accurate and realistic adaptation scenario should be defined based on physiological characteristics of human body as well as biological factors. It (at least) requires investigating the likely adaptation scenarios of human body during the past decades, which is beyond the scope of the current study. Albeit some studies have proposed theoretical adaptation scenarios (WHO, 2014), they fail to provide physically-based assessments. Therefore, researchers are encouraged to

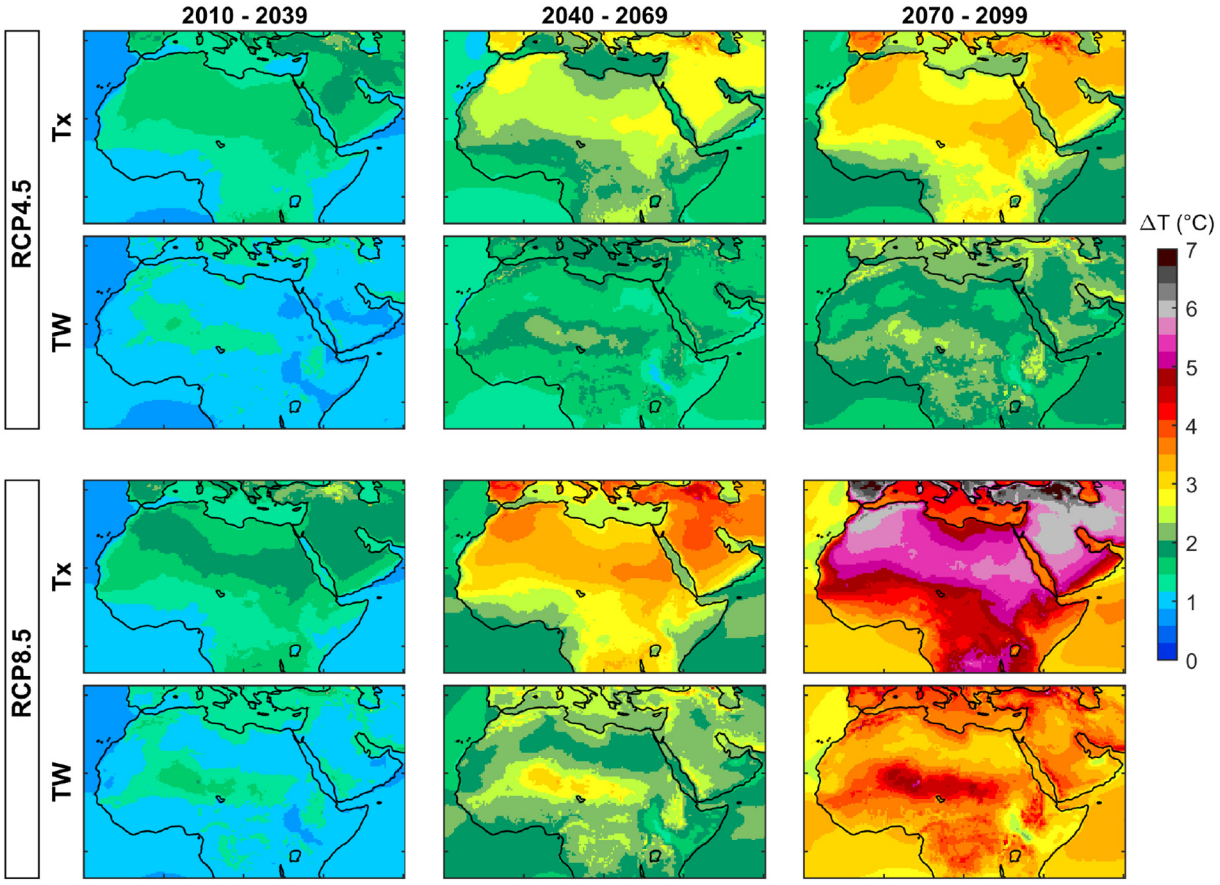

Fig. 6. Decadal mean changes of maximum near-surface air temperature (ΔTx) and wet-bulb temperature (ΔTW) for 30-year future periods. The figure is generated using the results of the ensemble mean of 17 RCMs.

assess the regional characteristics of air temperature and physiological attributes of human body to develop adaptation scenarios for further heat-related assessments.

Numerous studies have assessed the hydrological, environmental, or economic impacts of climate change (Ahmadalipour et al., 2017a, 2017b; Dai, 2012; Gosling and Arnell, 2016; Wang et al., 2017; Zhao and Dai, 2016). However, climate change impacts on human and livestock had received less attention. This study is the first attempt for implementing fine-resolution CORDEX RCMs to project the health impacts of a warming world. We showed that climate change will intensify extreme temperatures and heatwaves, which will in turn exacerbate mortality risk across MENA. The findings of the current study are in agreement with previous assessments and corroborate the need for urgent restriction and mitigation of climate change in order to attenuate future social and human-related impacts (Ciavarella et al., 2017; Lelieveld et al., 2016).

In the present study, daily maximum air temperature (i.e. the finest temporal resolution available from the CORDEX RCMs over Africa) was analyzed. Hence, it may not reflect the peak heat stress amplified by diurnal temperature cycles. Furthermore, our analysis applies to fully shaded conditions, as the effects of solar insolation and wind are neglected. Thus, for instance, the mortality risk for construction workers who work during the peak sunshine hours in a humid region is expected to be higher than that calculated here.

The health risk function (and subsequently the impacts of heatwaves on human body) is different for different locations, mainly due to the socioeconomic conditions, human adaptation capacity, primary occupation (field vs. indoor), population, age, infrastructure and air conditioning facilities, regional weather forecast accuracy and outreach, and medical facilities (Huber et al., 2017; Loughnan et al., 2010; Merte, 2017). Therefore, it is necessary to investigate regional mortality rates and develop accurate health risk models (Kjellstrom et al., 2016). Such assessments are usually carried out at regional domains and not at a global scale. The advancement of health risk models and joint efforts between climate and health researchers can significantly enhance the reliability and accuracy of climate change health impact assessments, and it will in turn be a useful evidence for facilitating climate change policy making and resiliency planning (Im et al., 2018; Li et al., 2016; Tebaldi and Wehner, 2018; WHO, 2014). The health-risk model used in this study has been evaluated for 32 cities around the globe, and it was proved to be accurate for global assessments (Honda et al., 2014).

The current study provided a probabilistic (and likely) assessment of the impacts of climate change on mortality risk at fine spatial resolution across a large domain, in order to encourage and emphasize the necessity of climate change mitigation and reducing net emissions. The results indicate the severity of mortality risk if no climate change planning is implemented (i.e. RCP8.5) versus if the global air temperature rise is limited to 2 °C (i.e. RCP4.5). The two future scenarios project vastly different mortality risk ratios in distant future, and it was demonstrated that the mortality risk in distant future will be at least 50% lower, if global warming is limited to 2 °C.

Numerous analyses have pointed out the benefits of limiting global warming and the severe environmental, economical, and social consequences of a warmer world (Sun et al., 2017; Underwood et al., 2017). According to recent analyses, it is still possible to limit the global warming to even < 2 °C by 2100 (Millar et al., 2017), albeit unlikely

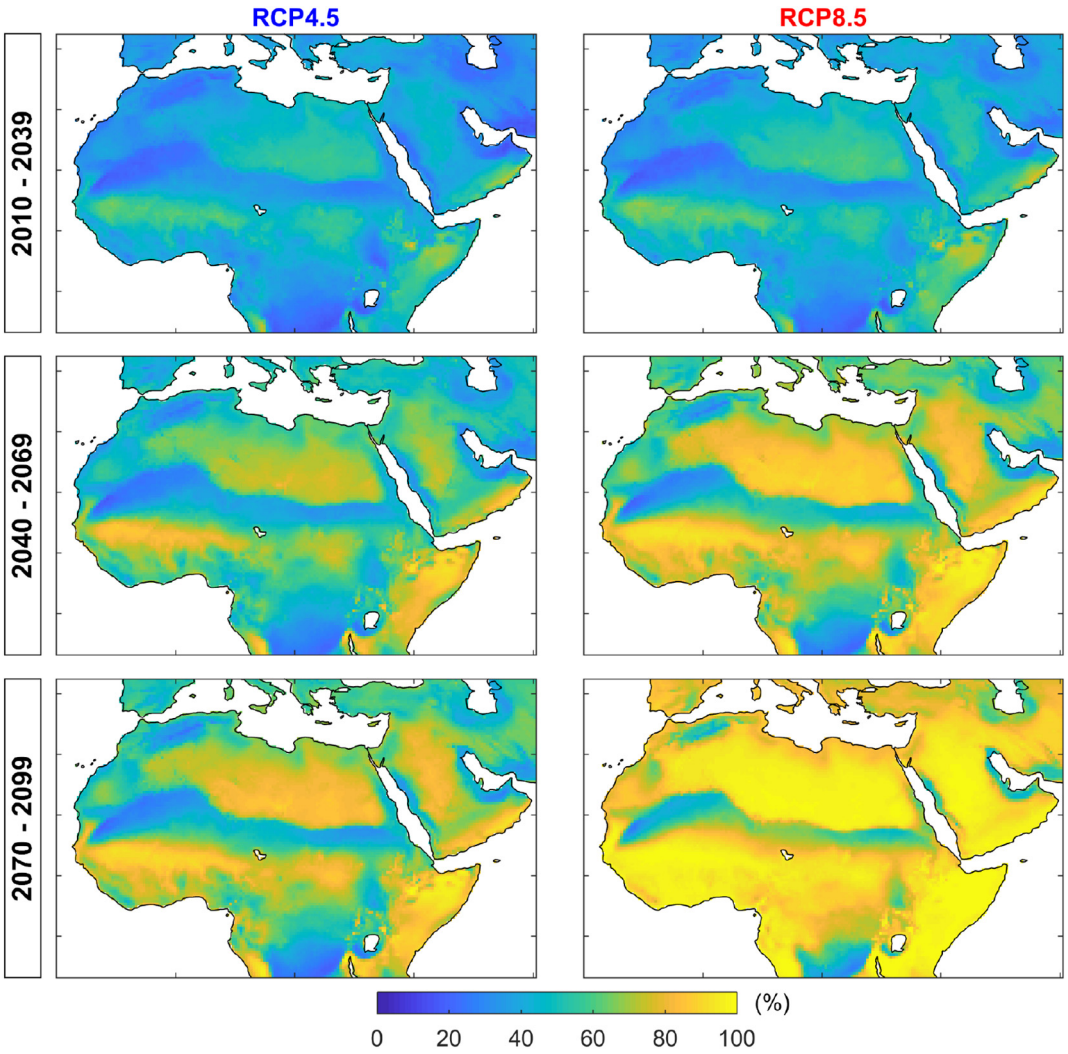

Fig. 7. The percentage of days with TW > T_{opt} (unsafe days) during each 30-year future period. The frequency is extracted for each RCM in each period, and the figure represents the ensemble mean of 17 RCMs.

(Raftery et al., 2017). The sooner the commitments are taken (and worked upon) to reduce net emissions to zero and stabilize climate, the higher the chance is to achieve the long-term temperature goal and mitigate the consequent climate change impacts and risks.

6. Summary and conclusion

In this study, daily maximum near-surface air temperature and humidity from 17 RCMs are utilized to quantify the impacts of climate change on mortality risk caused by excessive heat stress. A recently developed health risk model is employed to quantify mortality risk using a spatially dynamic optimum temperature threshold. The analysis is applied to the historical period of 1951–2005 and two future scenarios of RCP4.5 and RCP8.5 for the period of 2006–2100. The main findings of this study are summarized as follows:

- The fine-resolution CORDEX RCMs accurately capture regional land cover and elevation effects on mortality risk.
- ΔTx and ΔTW (changes of dry- and wet-bulb temperature) show linear relationship over water. Whereas over land, ΔTx is always higher than ΔTW.
- The highest (least probable) mortality risk ratio from RCP4.5 is lower than the median (most probable) mortality risk projected by RCP8.5 in distant future, which emphasizes the necessity of climate change mitigation.
- The coastal regions of the Red sea, Persian Gulf, and the Mediterranean Sea indicate substantial increase of mortality risk.
- The mortality risk ratio shows a similar latitudinal pattern over time, and the 12°N latitude indicates the highest increase of mortality among others, with the highest uncertainty.

Acknowledgement

We acknowledge the Centre for Environmental Data Analysis (CEDA) for providing access to CRU observations, the European Centre for Medium Range Weather Forecasts (ECMWF) for the ERA-interim dataset, and the Coordinated Regional Climate Downscaling Experiment (CORDEX) for RCMs.

Appendix A. Supplementary information

Supplementary data to this article can be found online at https://doi.org/10.1016/j.envint.2018.05.014.

References

Ahmadalipour, A., Moradkhani, H., Demirel, M.C., 2017a. A comparative assessment of projected meteorological and hydrological droughts: elucidating the role of temperature. J. Hydrol. 553, 785–797. http://dx.doi.org/10.1016/j.jhydrol.2017.08.047.

Ahmadalipour, A., Moradkhani, H., Svoboda, M., 2017b. Centennial drought outlook over the CONUS using NASA-NEX downscaled climate ensemble. Int. J. Climatol. 37, 2477–2491. http://dx.doi.org/10.1002/joc.4859.

Ahmadalipour, A., Moradkhani, H., Rana, A., 2018. Accounting for downscaling and model uncertainty in fine-resolution seasonal climate projections over the Columbia River basin. Clim. Dyn. 50, 717–733. http://dx.doi.org/10.1007/s00382-017-3639-4.

Chen, K., Horton, R.M., Bader, D.A., Lesk, C., Jiang, L., Jones, B., Zhou, L., Chen, X., Bi, J., Kinney, P.L., 2017. Impact of climate change on heat-related mortality in Jiangsu Province, China. Environ. Pollut. 224, 317–325.

Christidis, N., Jones, G.S., Stott, P.A., 2015. Dramatically increasing chance of extremely hot summers since the 2003 European heatwave. Nat. Clim. Chang. 5, 46–50.

Ciavarella, A., Stott, P., Lowe, J., 2017. Early benefits of mitigation in risk of regional climate extremes. Nat. Clim. Chang. 7, 326–330.

Coffel, E.D., Horton, R.M., de Sherbinin, A., 2017. Temperature and humidity based projections of a rapid rise in global heat stress exposure during the 21st century. Environ. Res. Lett. 13, 14001.

Dai, A., 2012. Increasing drought under global warming in observations and models. Nat. Clim. Chang. 3, 52–58.

Dee, D.P., Uppala, S.M., Simmons, A.J., Berrisford, P., Poli, P., Kobayashi, S., Andrae, U., Balmaseda, M.A., Balsamo, G., Bauer, P., 2011. The ERA-Interim reanalysis: configuration and performance of the data assimilation system. Q. J. R. Meteorol. Soc. 137, 553–597.

Dosio, A., 2016. Projection of temperature and heat waves for Africa with an ensemble of CORDEX Regional Climate Models. Clim. Dyn. 1–27.

Dunne, J.P., Stouffer, R.J., John, J.G., 2013. Reductions in labour capacity from heat stress under climate warming. Nat. Clim. Chang. 3, 563–566.

Etemadi, H., Samadi, S., Sharifikia, M., 2013. Uncertainty analysis of statistical downscaling models using general circulation model over an international wetland. Clim. Dyn. 42, 2899–2920. http://dx.doi.org/10.1007/s00382-013-1855-0.

Fischer, E.M., Knutti, R., 2015. Anthropogenic contribution to global occurrence of heavy-precipitation and high-temperature extremes. Nat. Clim. Chang. 5, 560–564.

Fischer, E.M., Beyerle, U., Knutti, R., 2013. Robust spatially aggregated projections of climate extremes. Nat. Clim. Chang. 3, 1033.

Gosling, S.N., Arnell, N.W., 2016. A global assessment of the impact of climate change on water scarcity. Clim. Chang. 134, 371–385.

Hameed, M., Ahmadalipour, A., Moradkhani, H., 2018. Apprehensive drought characteristics over Iraq: results of a multidecadal spatiotemporal assessment. Geosciences 8, 58.

Harris, I., Jones, P.D., Osborn, T.J., Lister, D.H., 2014. Updated high-resolution grids of monthly climatic observations–the CRU TS3. 10 dataset. Int. J. Climatol. 34, 623–642.

Honda, Y., Kondo, M., McGregor, G., Kim, H., Guo, Y.-L., Hijioka, Y., Yoshikawa, M., Oka, K., Takano, S., Hales, S., 2014. Heat-related mortality risk model for climate change impact projection. Environ. Health Prev. Med. 19, 56–63.

Huber, V., Ibarreta, D., Frieler, K., 2017. Cold-and heat-related mortality: a cautionary note on current damage functions with net benefits from climate change. Clim. Chang. 1–12.

Im, E.-S., Pal, J.S., Eltahir, E.A.B., 2017. Deadly heat waves projected in the densely populated agricultural regions of South Asia. Sci. Adv. 3, e1603322.

Im, E.-S., Kang, S., Eltahir, E.A.B., 2018. Projections of rising heat stress over the western Maritime Continent from dynamically downscaled climate simulations. In: Glob. Planet. Change.

Jones, C., Giorgi, F., Asrar, G., 2011. The coordinated regional downscaling experiment: CORDEX–an international downscaling link to CMIP5. CLIVAR Exch. 56, 34–40.

Kam, J., Knutson, T.R., Zeng, F., Wittenberg, A.T., 2016. Multimodel assessment of anthropogenic influence on record global and regional warmth during 2015. Bull. Am. Meteorol. Soc. 97, S4–S8.

King, A.D., Karoly, D.J., Henley, B.J., 2017. Australian climate extremes at 1.5 °C and 2 °C of global warming. Nat. Clim. Chang. 7, 412–416.

Kingsley, S.L., Eliot, M.N., Gold, J., Vanderslice, R.R., Wellenius, G.A., 2016. Current and projected heat-related morbidity and mortality in Rhode Island. Environ. Health Perspect. 124, 460.

Kjellstrom, T., Briggs, D., Freyberg, C., Lemke, B., Otto, M., Hyatt, O., 2016. Heat, human performance, and occupational health: a key issue for the assessment of global climate change impacts. Annu. Rev. Public Health 37, 97–112.

Knutson, T.R., Ploshay, J.J., 2016. Detection of anthropogenic influence on a summertime heat stress index. Clim. Chang. 138, 25–39.

Lelieveld, J., Proestos, Y., Hadjinicolaou, P., Tanarhte, M., Tyrlis, E., Zittis, G., 2016. Strongly increasing heat extremes in the Middle East and North Africa (MENA) in the 21st century. Clim. Chang. 137, 245–260.

Lewis, S.C., Karoly, D.J., 2013. Anthropogenic contributions to Australia's record summer temperatures of 2013. Geophys. Res. Lett. 40, 3705–3709.

Li, T., Horton, R.M., Bader, D.A., Zhou, M., Liang, X., Ban, J., Sun, Q., Kinney, P.L., 2016. Aging will amplify the heat-related mortality risk under a changing climate: projection for the elderly in Beijing, China. Sci. Rep. 6, 28161.

Loughnan, M., Nicholls, N., Tapper, N., 2010. Mortality–temperature thresholds for ten major population centres in rural Victoria, Australia. Health Place 16, 1287–1290.

Loughnan, M., Nicholls, N., Tapper, N.J., 2012. Mapping heat health risks in urban areas. Int. J. Popul. Res. 2012.

Luo, L., Zhang, Y., 2012. Did we see the 2011 summer heat wave coming? Geophys. Res. Lett. 39, L09708.

Mazdiyasni, O., AghaKouchak, A., Davis, S.J., Madadgar, S., Mehran, A., Ragno, E., Sadegh, M., Sengupta, A., Ghosh, S., Dhanya, C.T., 2017. Increasing probability of mortality during Indian heat waves. Sci. Adv. 3, e1700066.

Merte, S., 2017. Estimating heat wave-related mortality in Europe using singular spectrum analysis. Clim. Chang. 142, 321–330.

Miao, C., Sun, Q., Kong, D., Duan, Q., 2016. Record-breaking heat in northwest China in July 2015: analysis of the severity and underlying causes. Bull. Am. Meteorol. Soc. 97, S97–S101.

Millar, R.J., Fuglestvedt, J.S., Friedlingstein, P., Rogelj, J., Grubb, M.J., Matthews, H.D., Skeie, R.B., Forster, P.M., Frame, D.J., Allen, M.R., 2017. Emission budgets and pathways consistent with limiting warming to 1.5 °C. Nat. Geosci. 10, 741–747. http://dx.doi.org/10.1038/ngeo3031.

Mitchell, D., 2016. Human influences on heat-related health indicators during the 2015 Egyptian heat wave. Bull. Am. Meteorol. Soc. 97, S70–S74.

Mitchell, D., Heaviside, C., Vardoulakis, S., Huntingford, C., Masato, G., Guillod, B.P., Frumhoff, P., Bowery, A., Wallom, D., Allen, M., 2016. Attributing human mortality during extreme heat waves to anthropogenic climate change. Environ. Res. Lett. 11, 74006.

Mora, C., Dousset, B., Caldwell, I.R., Powell, F.E., Geronimo, R.C., Bielecki, C.R., Counsell, C.W.W., Dietrich, B.S., Johnston, E.T., Louis, L.V., 2017. Global risk of deadly heat. Nat. Clim. Chang. 7, 501–506.

Nikiema, P.M., Sylla, M.B., Ogunjobi, K., Kebe, I., Gibba, P., Giorgi, F., 2017. Multi-model CMIP5 and CORDEX simulations of historical summer temperature and precipitation variabilities over West Africa. Int. J. Climatol. 37, 2438–2450.

Ostro, B., Barrera-Gómez, J., Ballester, J., Basagaña, X., Sunyer, J., 2012. The impact of future summer temperature on public health in Barcelona and Catalonia, Spain. Int. J. Biometeorol. 56, 1135–1144.

Pal, J.S., Eltahir, E.A.B., 2016. Future temperature in southwest Asia projected to exceed a threshold for human adaptability. Nat. Clim. Chang. 6, 197–200.

Peng, R.D., Bobb, J.F., Tebaldi, C., McDaniel, L., Bell, M.L., Dominici, F., 2011. Toward a quantitative estimate of future heat wave mortality under global climate change. Environ. Health Perspect. 119, 701.

Raftery, A.E., Zimmer, A., Frierson, D.M.W., Startz, R., Liu, P., 2017. Less than 2 °C warming by 2100 unlikely. Nat. Clim. Chang. 7, 637–641. http://dx.doi.org/10.1038/nclimate3352.

Rana, A., Moradkhani, H., 2016. Spatial, temporal and frequency based climate change assessment in Columbia River Basin using multi downscaled-scenarios. Clim. Dyn. 47, 579–600.

Rana, A., Moradkhani, H., Qin, Y., 2017. Understanding the joint behavior of temperature and precipitation for climate change impact studies. Theor. Appl. Climatol. 129, 321–339.

Raymond, C., Singh, D., Horton, R.M., 2017. Spatiotemporal patterns and synoptics of extreme wet-bulb temperature in the contiguous United States. J. Geophys. Res. Atmos. 122, 13,108–13,124.

Ring, C., Pollinger, F., Kaspar-Ott, I., Hertig, E., Jacobeit, J., Paeth, H., 2017. A comparison of metrics for assessing state-of-the-art climate models and implications for probabilistic projections of climate change. Clim. Dyn. 1–20.

Ross, M.E., Vicedo-Cabrera, A.M., Kopp, R.E., Song, L., Goldfarb, D.S., Pulido, J., Warner, S., Furth, S.L., Tasian, G.E., 2018. Assessment of the combination of temperature and relative humidity on kidney stone presentations. Environ. Res. 162, 97–105.

Russo, S., Marchese, A.F., Sillmann, J., Immé, G., 2016. When will unusual heat waves become normal in a warming Africa? Environ. Res. Lett. 11, 54016.

Schär, C., 2016. Climate extremes: the worst heat waves to come. Nat. Clim. Chang. 6, 128–129.

Stull, R., 2011. Wet-bulb temperature from relative humidity and air temperature. J. Appl. Meteorol. Climatol. 50, 2267–2269.

Sun, Y., Zhang, X., Zwiers, F.W., Song, L., Wan, H., Hu, T., Yin, H., Ren, G., 2014. Rapid increase in the risk of extreme summer heat in eastern China. Nat. Clim. Chang. 4, 1082–1085.

Sun, Q., Miao, C., AghaKouchak, A., Duan, Q., 2017. Unraveling anthropogenic influence on the changing risk of heat waves in China. Geophys. Res. Lett. 44, 5078–5085.

Tebaldi, C., Wehner, M.F., 2018. Benefits of mitigation for future heat extremes under RCP4. 5 compared to RCP8. 5. Clim. Chang. 146, 349–361.

Underwood, B.S., Guido, Z., Gudipudi, P., Feinberg, Y., 2017. Increased costs to US pavement infrastructure from future temperature rise. Nat. Clim. Chang. 7 (10), 704.

Waha, K., Krummenauer, L., Adams, S., Aich, V., Baarsch, F., Coumou, D., Fader, M., Hoff, H., Jobbins, G., Marcus, R., 2017. Climate change impacts in the Middle East and Northern Africa (MENA) region and their implications for vulnerable population groups. Reg. Environ. Chang. 17, 1623–1638.

Wang, Y., Sun, Y., Hu, T., Qin, D., Song, L., 2017. Attribution of temperature changes in Western China. Int. J. Climatol. 38, 742–750.

Weinberger, K.R., Haykin, L., Eliot, M.N., Schwartz, J.D., Gasparrini, A., Wellenius, G.A., 2017. Projected temperature-related deaths in ten large US metropolitan areas under different climate change scenarios. Environ. Int. 107, 196–204.

WHO, 2014. Quantitative Risk Assessment of the Effects of Climate Change on Selected

Causes of Death, 2030s and 2050s. World Health Organization.
Willett, K.M., Sherwood, S., 2012. Exceedance of heat index thresholds for 15 regions under a warming climate using the wet-bulb globe temperature. Int. J. Climatol. 32, 161–177.
Williams, S., Nitschke, M., Weinstein, P., Pisaniello, D.L., Parton, K.A., Bi, P., 2012. The impact of summer temperatures and heatwaves on mortality and morbidity in Perth, Australia 1994–2008. Environ. Int. 40, 33–38.
Zander, K.K., Botzen, W.J.W., Oppermann, E., Kjellstrom, T., Garnett, S.T., 2015. Heat stress causes substantial labour productivity loss in Australia. Nat. Clim. Chang. 5, 647–651.
Zhao, T., Dai, A., 2016. Uncertainties in historical changes and future projections of drought. Part II: model-simulated historical and future drought changes. Clim. Chang. 1–14.
Zhao, Y., Sultan, B., Vautard, R., Braconnot, P., Wang, H.J., Ducharne, A., 2016. Potential escalation of heat-related working costs with climate and socioeconomic changes in China. Proc. Natl. Acad. Sci. 113, 4640–4645.